Research & Reviews: Journal of Material Sciences e-ISSN: 2321-6212

Dynamic Stiffness Control: An Approach Utilizing Heuristics

Farhad Fakour[1] and M. Hossein Siadati[2*]

[1]Department of Material Sciences, Haas Automation Inc., Oxnard, California, USA

[2]Department of Material Sciences, K. N. Toosi University of Technology, Tehran, Iran

Research Article

Received: 06-Mar-2023, Manuscript No. JOMS-23-90959; **Editor assigned:** 08-Mar-2023, PreQC No. JOMS-23-90959 (PQ); **Reviewed:** 22-Mar-2023, QC No. JOMS-23-90959; **Revised:** 29-Mar-2023, Manuscript No. JOMS-23-90959 (R);**Published:** 05-Apr-2023, DOI: 10.4172/2321-6212.11.3.002.

***For Correspondence:**
M. Hossein Siadati, Department of Material Sciences, K. N. Toosi University of Technology, Tehran, Iran

E-mail: siadati@kntu.ac.ir

Citation: Fakour F, et al. Dynamic Stiffness Control: An Approach Utilizing Heuristics. RRJ Mater Sci. 2023;11:002.

ABSTRACT

For appropriate and even superior performance yet cost reduction, this work was performed with the aim of weight reduction in the overall design and construction of possibly any machine tools. As far as our literature search is concerned, there does not seem to be much work published regarding successful weight reduction while maintaining performance using Mass Participation Factor (MPF) in the areas of interest of the machine tools. In order to accomplish this task, we started with the 'bed' compartment of a CNC system and resorted to using the Finite Element Analysis (FEA) software package and thoughtfully manipulated the available data/parameters until the desired results were obtained. The most important parameters were static stiffness, dynamic stiffness, and damping ratio. On the 'bed' of the machines' compartment currently in production, it was so identified that there was unnecessary material (dead weight), and thus the FEA software was used in order to remove the unnecessary material by iteration. Finally, a new machine was built devoid of the unnecessary material, resulted in 9.3% weight reduction as predicted by the simulation, without sacrificing any accuracy and/or precision in performance.

Keywords: Static/dynamic stiffness control; Mass participation factor; Finite element analysis; Weight reduction; Machine

INTRODUCTION

Considering the importance of smooth and precise manufacturing, there have been continuous attempts in upgrading machine tools for enhancing their performance, weight reduction, and of course, cost minimization. Various aspects of optimization have been considered such as computer-aided engineering [1] or genetic algorithm [2], or grey relational analysis [3], or by load-bearing topology [4] or even by a biologically inspired topology optimization method [5], and also on static and dynamic characteristics [6-8], for lathe-bed [9,10] or vertical milling machines [11,12]. Also, weight reduction by using composite materials [13], or by shape optimization using static stiffness optimization have been considered [14]. However, very few attempts have focused on using Mass Participation Factor (MPF) to achieve machine optimization [15,16]. The mathematics of MPF has also been reported [17], however, to the best of our knowledge, no attempt has been undertaken to compare the simulation results to the experimental results.

In this study, we used MPF in the areas of interest of a machine currently in production to minimize/eliminate the unnecessary material (dead weight) in constructing a new machine. Indeed, a new machine with 9.2% less weight was constructed based on the simulation results, and the iterations involved. For this purpose, the following activities were conducted.

MATERIALS AND METHODS

FEA static analysis

Static stiffness: For start, a model was created in the Solid Modeller software. Then, to analyse the model, it was transferred to the FEA software. During the analysis, the model was first constrained from some specific sites on the model (constraint sites) as shown with color green in Figure 1.

Figure 1. Starting model showing the areas of interest and the constraint sites (green color).

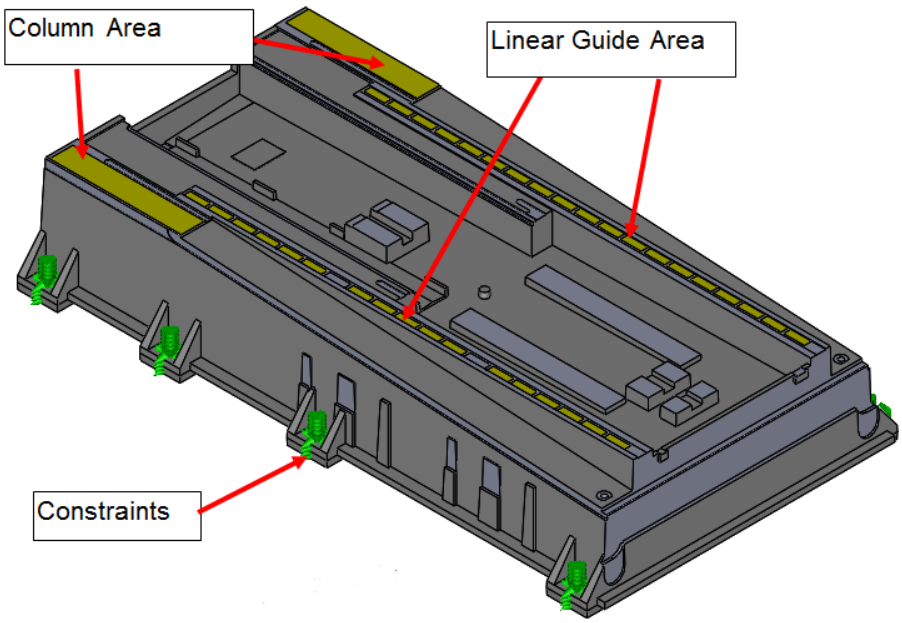

Then forces in the X-axis were applied onto some specific areas of the constrained model to obtain the ratio of force over deflection in order to determine the static stiffness in the X-axis for each specific area a force was applied. The same was

applied in the Y-axis, and then to the Z-axis followed by determining the static stiffness for each specific area the force was applied.

FEA modal analysis

Unconstrained modal analysis: The structure may contain a number of local modes in vibration, and identifying them is of great importance [16]. The first few modes are called rigid modes (translational). The rigid modes have extremely low frequency and are of not much interest in this study. It is important to note that the first twisting mode is of special interest in this heuristic technique due to the inherent occurrence of its frequency and modal shape. The first twisting mode is also known as non-rigid mode. Of considerable importance is the fact that this twisting mode is at the centre of gravity whose MPF is the least as shown with blue colour in the bed of the production machine (Figure 2). In the complex system of machine tools, the bed is a very important part because its layout and dimensions affect the dynamic performance of the entire machine [16].

Figure 2. The bed of the production machine showing MPF in blue color.

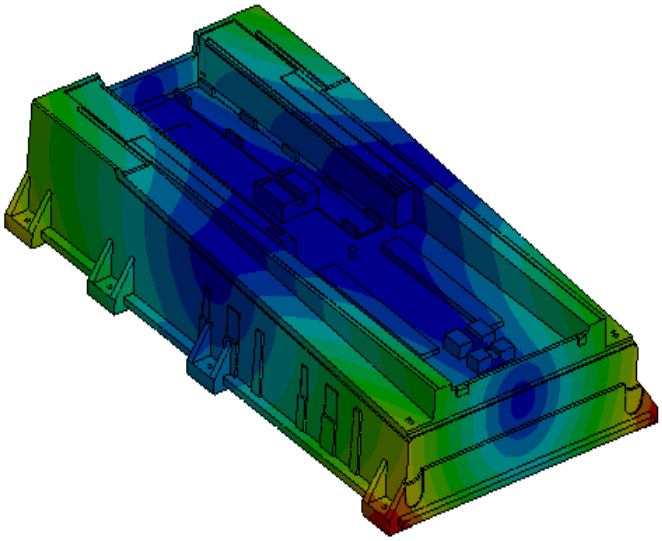

On the other hand, the areas with the largest MPF are shown with red color in Figure 2. It is important to note that MPF involves the mass that causes vibration with some frequency (23 Hz). In other words, the MPF associated with each mode represents the amount of system mass participating in that mode. If the value associated with MPF is small, it indicates that there is little vibration in that particular area, and vice versa.

Constrained modal analysis: The same constraints as in the static analysis apply in this section, too. The constraint sites as presented in green color, along with the first 5 modes and their corresponding MPF are shown in Figure 3a. The scheme of the original simulated model ('bed' compartment currently in production, referred to as the production bed here on) is shown in Figure 3a and the new simulated model shown in Figure 3b (the bed with weight reduction, referred to as the new bed here on). The darker blue in Figure 3b illustrates the first twisting mode; it is superior for its smaller amplitude (Figures 3a and 3b).

Figure 3a. The simulated model for the production bed, for the first mode, showing constraint sites in green color.

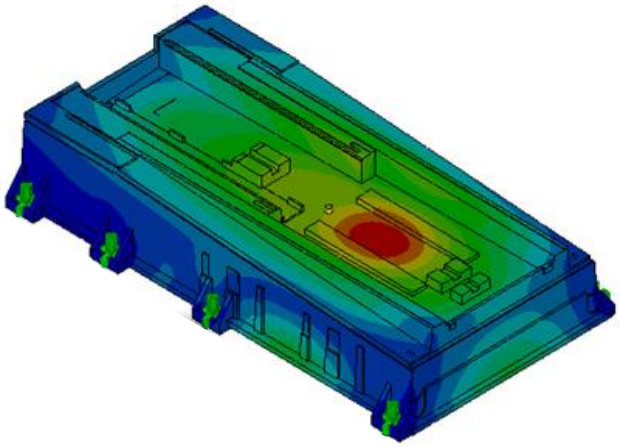

Figure 3b. The simulated model for the new bed highlighting the first twisting mode in darker blue; it is superior because it has smaller amplitude.

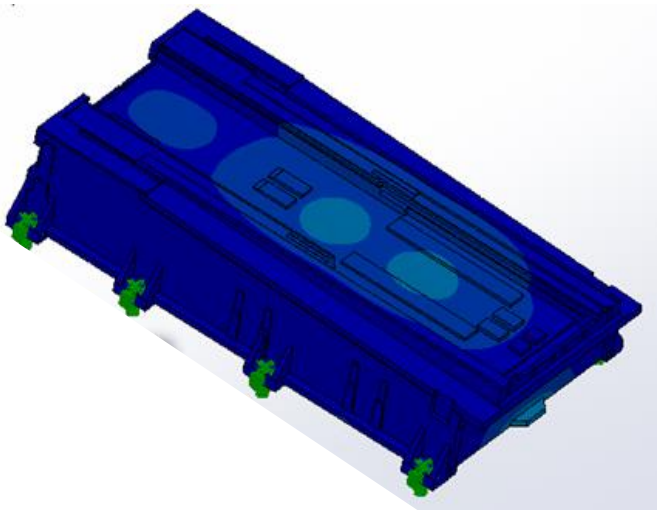

The frequencies and modal shapes of the first 5 modes are important; the first mode being the most important. Among these five, the first mode inherently has the lowest frequency (144 Hz, Figure 3a). The challenge is to modify by iterations, and thus to minimize the MPF of the first mode in the areas of interest on the new bed (151 Hz Figure 3b). It is important to note that the localities of the areas of interest remain the same throughout the entire simulation.

Furthermore, the MPF minimization at areas of interest will be achieved without sacrificing the static stiffness in all 3 axes. At the same time, we have succeeded in reducing or minimizing the mass of the part/machine. For instance, in this study, the total mass reduction for the part in Figure 3a is 9%. Along with mass reduction, achieving the least MPF is desirable because it shows the best characteristics of the created/developed model. In a similar MPF simulation study, by raising the natural frequency, the weight of the bed was reduced by 4.8% [16].

FEA dynamic analysis

Harmonic analysis: In order to study the dynamic stiffness, harmonic analysis was performed. While the information provided by dynamic analysis are displacement, velocity, and acceleration, in this study, we were interested in studying the displacement only. It is known that the results from harmonic analysis confirm the effects of MPF at any particular area of interest by studying the amplitude of dynamic displacement. The size of amplitude determines the magnitude of dynamic stiffness at any particular mode; the smaller the amplitude, the larger the dynamic stiffness. As shown in Figure 4, the graphs compare the frequencies and amplitudes of the first modes for both the production and new models. It is obvious that the brown dash graph describing the new model shows a smaller amplitude at the first mode. Another important point is the fact that the two graphs are at different frequencies indicating better damping and dynamic stiffness for the new model. It is important to note that the same constraints and also 10% of the forces (same direction) as in the static analysis were applied in this harmonic analysis. Knowing that the smallest static stiffness is the worst, the harmonic analysis was done in the axis that showed the smallest static stiffness (Figure 4).

Figure 4. Comparing frequencies and amplitudes of the first modes of the production and the new models. **Note**: —— X in Production column area, - - - X in New column area.

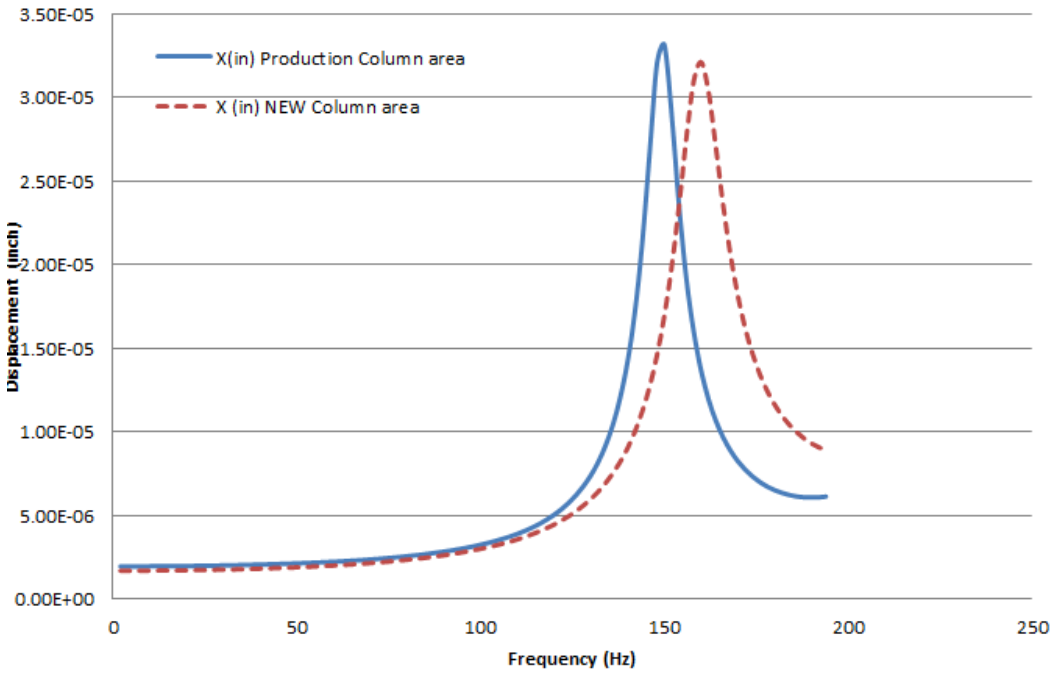

Experimental

Dynamic and modal tests were conducted to verity the simulation results. In order to do the tests, a 'bed' compartment based on the size and dimensions resulted by the new model was built. The new model was 9.3% (605 lb.) lighter than the production model. For comparison purposes, the experimental tests were conducted on both the production and the new 'bed' compartments.

Dynamic tests

Both 'bed' compartments were tested using two different test methods, the shaker test, and the modal (hammer) test.

Shaker test on the 'bed' compartment: For conducting the shaker test, a powerful centrifugal shaker was placed on the 'bed' compartment where the 'column' compartment sits. The amplitude and frequency of the vibrations experienced at four different sites on each linear guide at equidistant places from each other were captured by tri-accelerometer sensors. The software LabVIEW was used for data acquisition/analysis. As shown in Figure 5, the shaker and the two accelerometers attached to the left and right of the 'bed' compartment onto the contact surface of the linear guides are observed. The other three measurements were conducted by placing the accelerometers farther away from the 'column' compartment. It is important to note that each accelerometer captures vibrations in time domain of 10 seconds experienced in all 3 axes simultaneously (Figure 5).

Figure 5. The 'bed' compartment onto which a shaker and two accelerometers (one on each left and right linear guides) were attached.

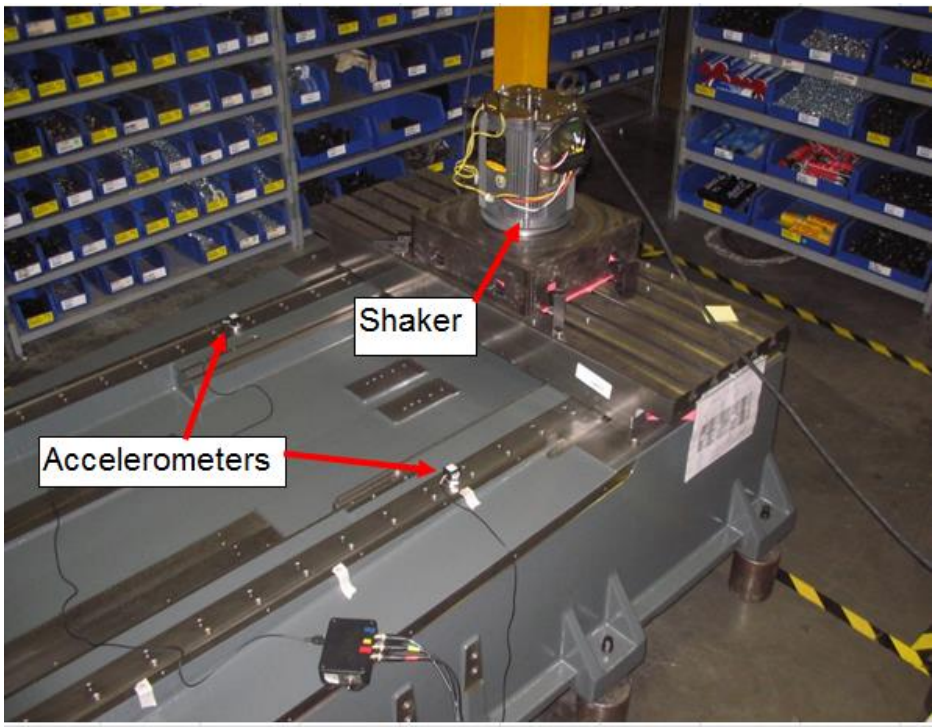

Modal (Hammer) test on the 'bed' compartment: For this test, a hammer was used to exert a force on a particular area of the 'bed' compartment and measure the vibration along the same axis as the force was exerted. In other words, when the force was exerted in the X-axis, the vibration in the X-axis was measured. Accelerometers were used for measuring the vibration. This was done identically for both 'bed' compartments, but the accelerometers were placed only on the left-hand side of the 'bed.' One accelerometer was used at a time and measured the vibrations in all 3 axes. The complete procedure for this test involving data acquisition/analysis was done using Data Physics software/hardware.

RESULTS AND DISCUSSION

Shaker test results

Figure 6 shows the vibration graphs for the left and the right linear guides of the production bed and the new bed in all 3 axes, as numerically presented in Tables 1a and 1b. The crucial features to observe in Figure 6 are the variations, in gravity unit (g=9.81 m^2/s), within the 3 axes as well as those in-between the two beds (production and new). For the production bed, as shown in Figure 6, the red and blue graphs illustrate the left side and the right side, respectively (Figure 6). One obvious point is the fact that MPF is large in both X and Y axes, while in the Z-axis, it is mostly low amplitude and thus not considerable. For instance, in Figure 6 and Table 1a, the variations in the X-axis from the left (0.016 g) to the right (0.018 g) linear guides indicate that they are not identically the same. This fact is also evident in the frequency domain (20 Hz) of the Fast Fourier Transform (FFT) graphs in Root Mean Square (RMS) values, 0.01130 *vs.* 0.01150, as shown in Table 1b.

Figure 6. Vibration graphs for the production bed in all 3 axes.

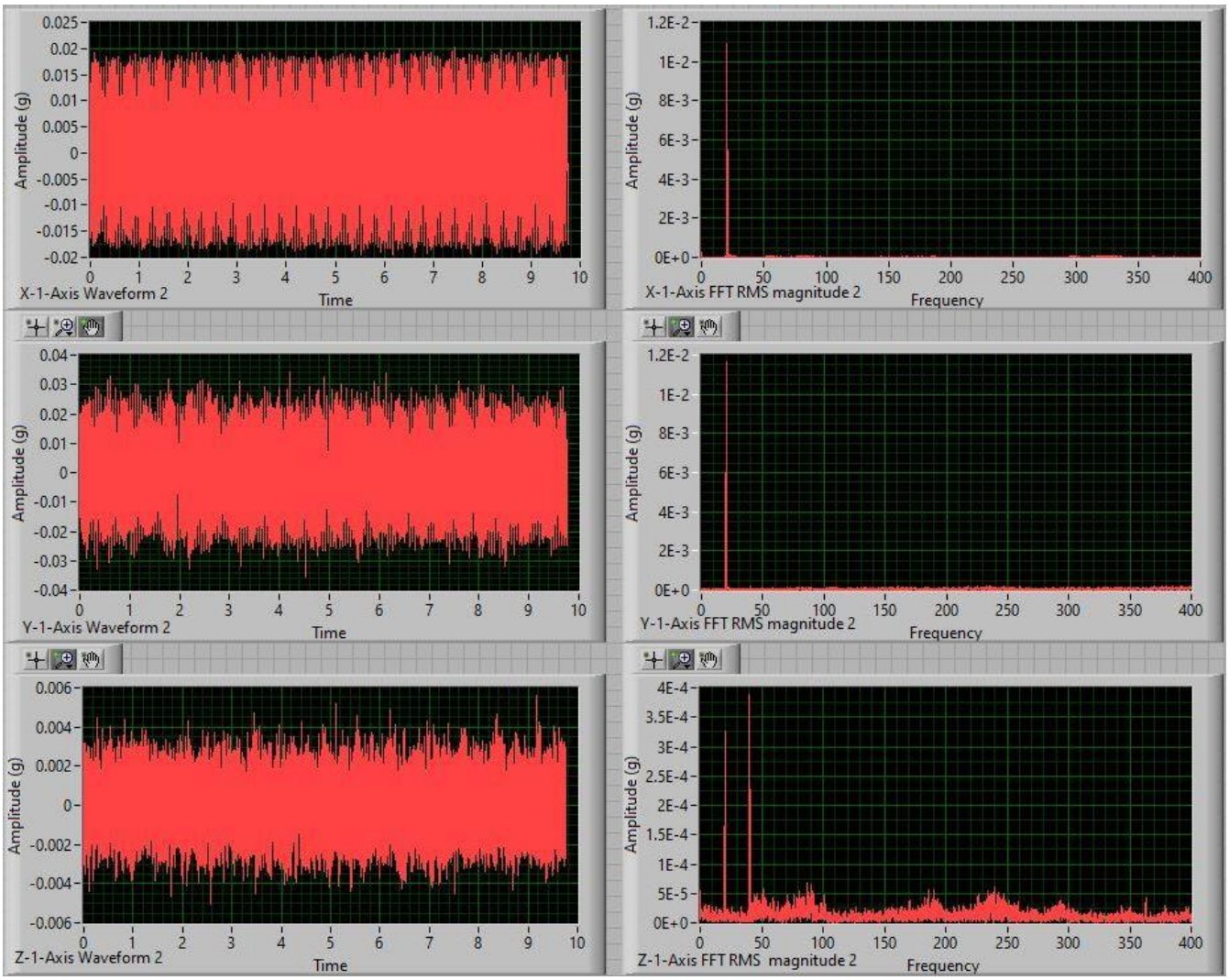

.

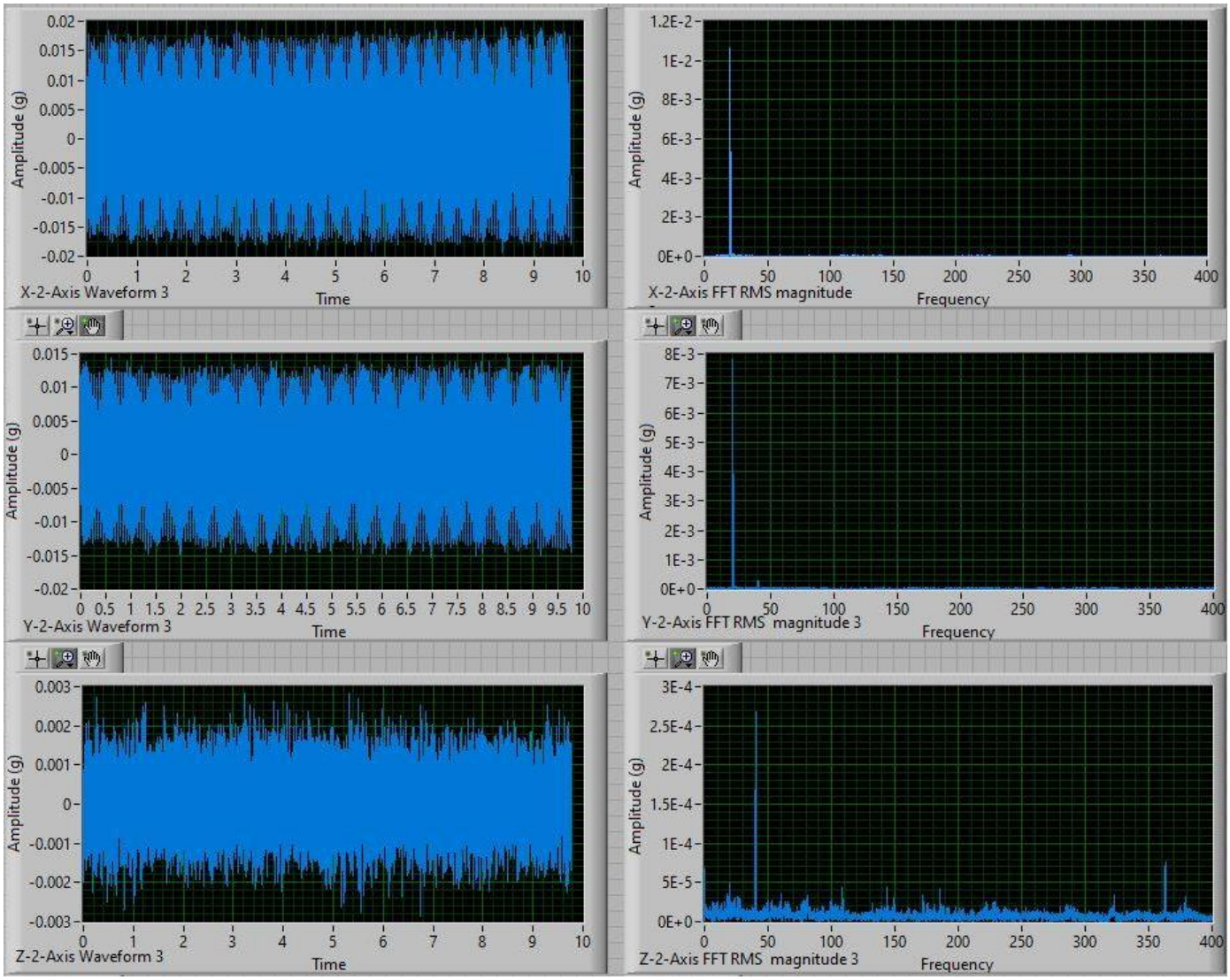

Furthermore, the improvement in the g values in-between the production bed and the new bed can also be observed. For instance, as shown in Table 1a, the variations in the Y-axis are (0.013 and 0.005) for the left side, and (0.025 and 0.010) for the right side; the improvement (more damping) is 0.008 and 0.015 for the left and the right sides, respectively. Moreover, the FFT values (Table 1b) indicate the same trend for the Y-axis at 20 Hz; (0.00780 and 0.00280) and (0.01200 and 0.00400) for the left and the right sides of the two beds; the improvement is 0.005 and 0.008 for the left and the right sides, respectively.

Table 1a. Time domain; comparison of variations between the two beds for all 3 axes.

Time domain	Left linear guide			Right linear guide		
	X	Y	Z	X	Y	Z
Production base (g)	0.016	0.013	0.0017	0.018	0.025	0.0035
New base (g)	0.013	0.005	0.001	0.013	0.01	0.0018
Delta (g)	0.003*	0.008*	0.0007*	0.005*	0.015*	0.0017*
Note: *=More damping.						

Table 1b. Frequency domain; comparison of variations between the two beds for all 3 axes.

Frequency domain (FFT)	Left (FFT) at 20 Hz			Right (FFT) at 20 Hz		
	X	Y	Z	X	Y	Z
Production base (g)	0.0113	0.0078	0.00003	0.0115	0.012	0.00038
New base (g)	0.008	0.0028	0.00019	0.0084	0.004	0.0004
Delta (g)	0.0033*	0.005*	-0.00016#	0.0031*	0.008*	-0.00002#
Note: #=Less damping and very insignificant magnitudes, *=More damping.						

In order to compare the variations with more ease, Figure 7 shows the variations superimposed in one graph for each side; the red and blue are for the production bed, onto which the white and green for the new bed are superimposed. The improvement is clearly visible (Figure 7).

Figure 7. Variations superimposed in one graph for each side.

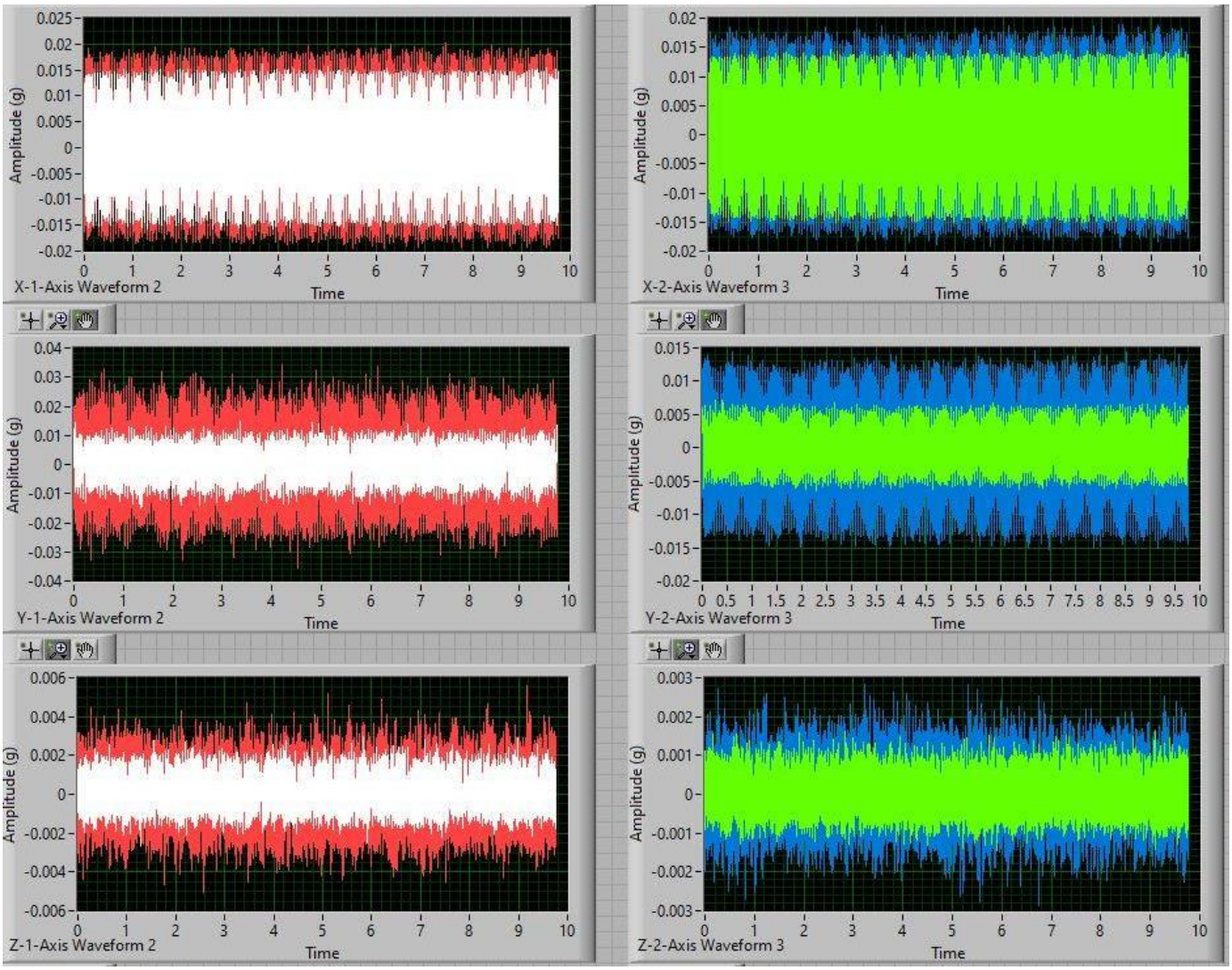

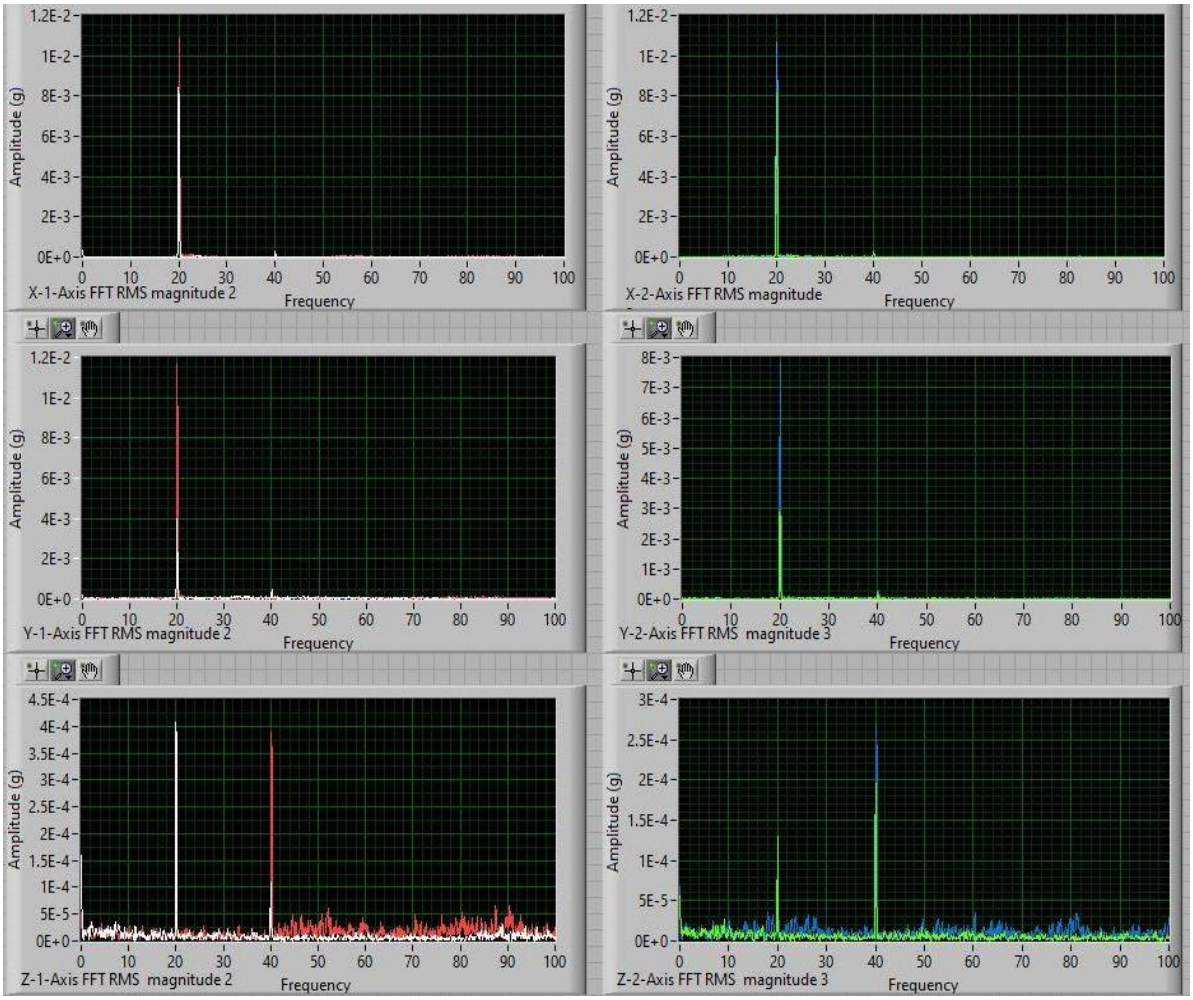

Although there are some negative results, as observed in Table 1b, the overall trend is positive from the production bed to the new bed compartment. Of course, the vital point is the fact that the overall results should be positive, and it is indeed the case in this study.

Modal test results

Figure 8 illustrates the transfer function graphs for the modal test on both 'bed' compartments. The Y-axis of the graph describes the ratio of output force over input force in the unit of gravity (g=9.81 m^2/s) over pound force (g/lbf). If this ratio is doubly integrated, it will provide the inverse of dynamic stiffness.

As shown in Figure 8 for the new bed, the first and second modes have higher dynamic stiffness, and also the roundness of the second mode demonstrates a higher damping ratio. The production bed has higher dynamic stiffness at the third mode (Figure 8).

Transfer function magnitude is inversely proportional to the dynamic stiffness; the smaller the magnitude, the larger the dynamic stiffness. Therefore, again in this particular case, the new bed is better. Table 2 gives the values of transfer function and frequency.

Table 2. Values of transfer function and frequency.

Below 50 Hz frequencies	Model 1		Model 2		Model 3	
Base (Hz)	12	11	16	14	38	43
Production base (g/lb)	0.00077	-	0.00187	-	-	0.00082
New base(g/lb)	-	0.00071*	-	0.00142*	0.00104#	-
Note: *=More damping, #=Less damping and very insignificant magnitudes.						

Figure 8. Transfer function graphs for the modal test on both 'bed' compartments. **Note**: New base, Production base.

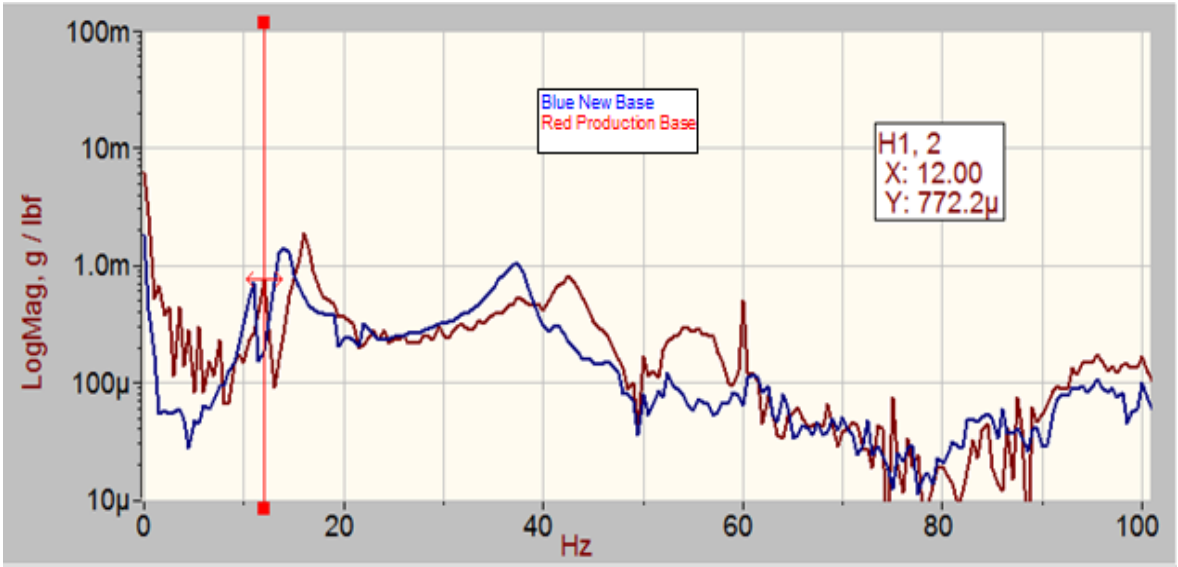

Another point was the frequency mismatch results between the modal test (17 Hz) and the FEA (144 Hz). In order to resolve this issue, levelling pads and screws were added to the FEA model and constraints were changed until correlation was achieved as shown in Figure 9. After this alteration in the FEA model, it resembled the real-world model very well (Figure 9).

Figure 9. Correlation was achieved after changing constraints.

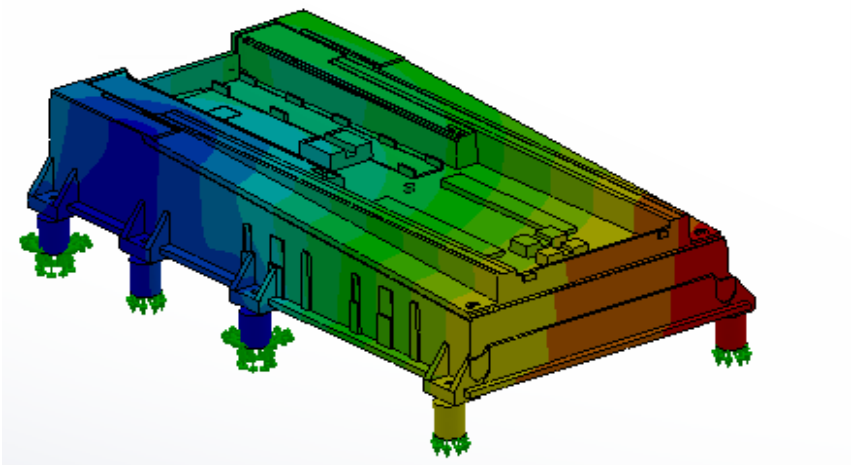

Performance evaluation

Dynamic analysis of machine (FEA): The two parts 'spindle' and 'table' were considered for harmonic testing. Figure 10 shows the FEA results of harmonic testing on both production and new machines for the X-axis. The peaks show the dynamic stiffness of the two beds. The solid blue curve shows the 'spindle,' and the solid brown shows the 'table' of the production machine, while the dashed red and blue curves show the 'table' of the new machine. Table 3 shows the excitation frequencies of the Y and Z axes, too (Figure 10).

Figure 10. FEA results of harmonic testing on both production and new machines, X-axis. **Note**: Production X spindle, Production X table, New X spindle, New X table.

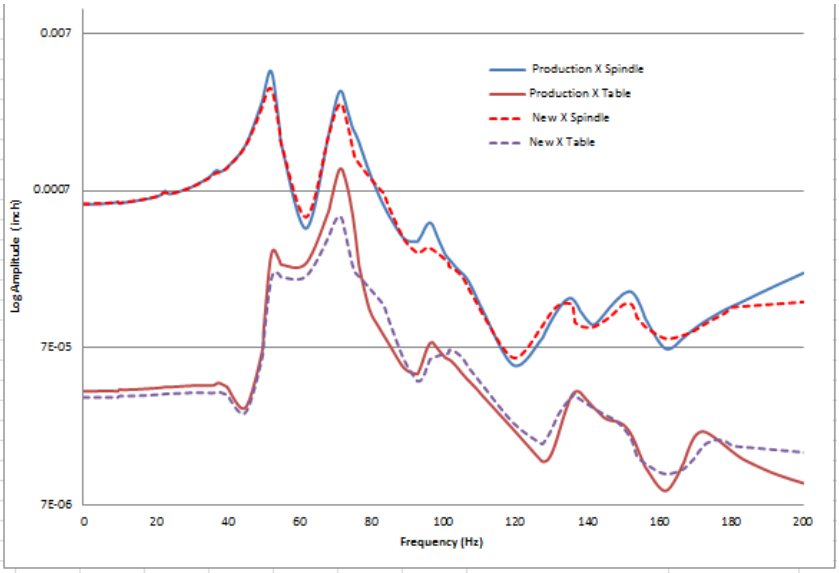

As for the production machine shown in Figure 10, 'spindle' mode 1 is at 23 Hz, mode 2 at 37 Hz, mode 3 at 52 Hz, and mode 4 at 71 Hz. The first two modes are tool changer frequencies, which are very small on the 'spindle.' Nevertheless, these two modes in case of jerk motion can create a ripple or texture mark on the side wall of the test cut. Mode 3 at 52 Hz and mode 4 at 71 Hz are actual main modes of machine casting/frame, and the new machine should have higher dynamic stiffness than the production one at the above-mentioned frequencies since the dashed red curve is smaller than the solid blue curve of the production machine. The production machine 'table' mode 1 is at 52 Hz and mode 2 at 71 Hz. The new machine should have higher dynamic stiffness than the production machine at the frequencies mentioned above since the dashed green curve is smaller than the solid red curve of the production machine. Important to note that the 'spindle' and 'table' frequencies match entirely. The frequency overlap is a potential bottleneck for any machine. The excitation frequencies of other axes are presented in Table 3.

Table 3. First mode amplitude (in) for all 3 axes.

Max up to 200 Hz	X axis	Y axis	Z axis
Production machine 'spindle'	0.00405	0.00162	0.003
Production machine 'table'	0.00097	0.0006	0.00067
New machine 'spindle'	0.00314*	0.00133*	0.00236*
New machine 'table'	0.00048*	0.00057*	0.00038*
Note:*=More damping.			

Modal (Hammer) test on 'spindle' and 'table': This test was done on both the production and the new machines (Figures 11a-11c). A hammer was used to exert a force on 'spindle' and 'table' and measured the vibrations along the same axis the force was exerted. Figures 11a-11c illustrates the transfer function graphs for the modal test on both 'spindle' and 'table.'

Figure 11a. Transfer function graphs for modal tests from Data Physics for both production bed and new bed. **Note:** New base, Production base.

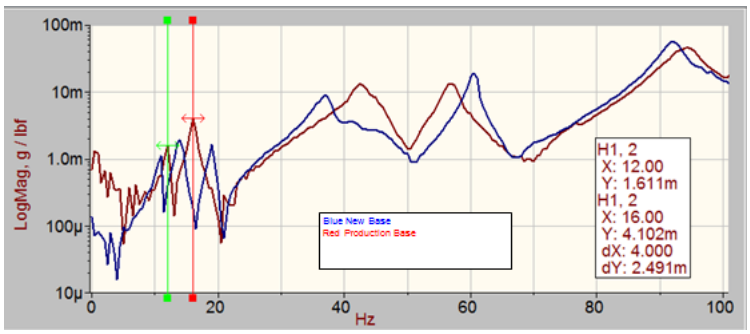

Figure 11b. Transfer function graphs for the modal test on 'spindle'. **Note**: Production machine spindle, New machine spindle.

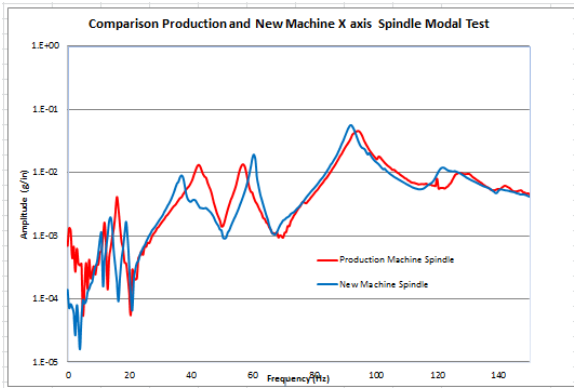

Figure 11c. Transfer function graphs for the modal test on 'table'. **Note:** Production machine table, New machine table.

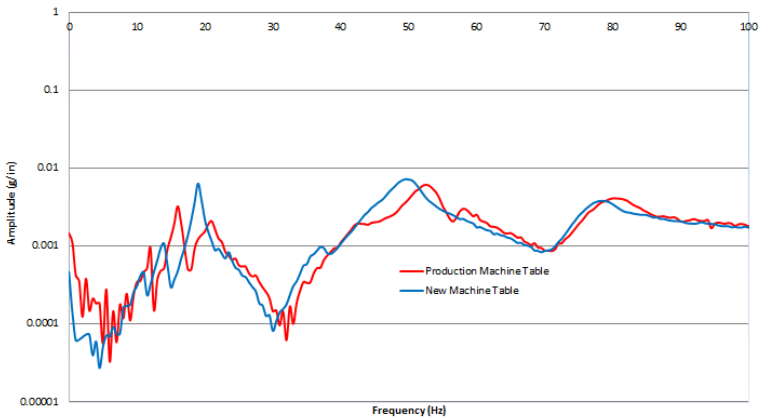

The production machine spindle's first 3 modes occur at frequencies of 12 Hz, 16 Hz, 37 Hz, and 59 Hz at amplitudes of 1.6, 4.1, 1.3, and 1.2 × 10^{-3} g/lbf, respectively. The new machine spindle's first 4 modes occur at 11, 14, 19, 37, and 60 Hz at 1.1, 1.9, 0.9 and 1.9 × 10^{-3} g/lbf, respectively. The values of amplitude in 3-axes for both 'spindle' and 'table' are given in Tables 4a and 4b.

Table 4a. Values of amplitude in 3-axes for 'spindle'.

Spindle								
Axes	**Model 1**		**Model 2**		**Model 3**		**Model 4**	
Machine (Hz)	12	11	16	14	37	37	59	60
Production base (g/lb)	0.0016	-	0.0041	-	0.0132	-	0.0122	-
New base(g/lb)	-	0.0011*	-	0.0019*	-	0.009*	-	0.019#
Note: *=More damping, #=Less damping and very insignificant magnitudes.								

Table 4b. Values of amplitude in 3-axes for 'table'.

Table										
Axes	**Model 1**		**Model 2**		**Model 3**		**Model 4**		**Model 5**	
Machine (Hz)	12	11	16	14	21	19	52	50	79	78
Production base (g/lb)	0.0009	-	0.0032	-	0.0021	-	0.0061	-	0.0038	-
New base(g/lb)	-	0.0005*	-	0.0011*	-	0.0063#		0.0072#	-	0.0038
Note: *=More damping, #=Less damping and very insignificant magnitudes.										

The amplitudes of all modes of the new machine 'spindle' up to the frequency of interest (50 Hz) are smaller compared to those of the production machine. As it was mentioned earlier, transfer function magnitude is inversely proportional to the dynamic stiffness; the smaller the magnitude, the larger the dynamic stiffness. In Figure 11b, it is clear that the first two modes have shorter amplitude while the third one has a higher amplitude, overall better because usually, the first two modes are the most important for machine structural stability.

Performance verification

To verify the performance of the new machine, cutting test was applied under the same conditions including rpm, feed rate (in/min), and tool path, which define the final shape. In this test, the production and the new machines were used to cut identical parts, and observed the surface finish and texture qualities of the machined parts for any differences. The final results portrayed no noticeable differences at all. It is important to note that in a simulation study, by adding ribs at suitable locations, 1.5% weight reduction was achieved [11], and in yet another study, using cross and horizontal ribs with hollow bed, the results indicated 4% weight reduction [6], but in this study, the weight reduction was 9.3% and it was experimentally verified. It was earlier mentioned that in a similar MPF simulation study, the weight of the bed was reduced by 4.8% [16].

CONCLUSION

We used the FEA software package to simulate weight reduction using MPF in the areas of interest while maintaining performance. We first applied the simulation to the 'bed' compartment, then extended it to the entire machine, and observed better results overall. Then, based on the simulation results, we constructed a new machine and tested it using the modal (hammer) test, and the test showed better results in the new machine as compared to the machines currently

in production. Finally, to evaluate their cutting accuracy and precision, the same pieces were cut using both the new and the production machines, and observed no significant difference in performance; in other words, the new machine with 9.3% reduced weight performed just as well as the production machine.

ACKNOWLEDGEMENT

We confirm that this work is original and has not been published elsewhere, nor is it currently under consideration for publication elsewhere. The authors declare that they have no known competing financial interests or personal relationships that could have appeared to influence the work reported in this paper.

DECLARATIONS

Funding

This research was non-financially supported by Haas Automation Inc., Oxnard, CA, USA.

Conflicts of interest

There are none.

Availability of data and material

There are none.

Code availability

Not applicable.

Ethics approval

Not applicable.

Consent to participate

Not applicable.

Consent for publication

The authors give their full consent for the publication of this article in this journal.

Authors' contributions

The original thought was devised by Farhad Fakour, and the manuscript preparation by Hossein Siadati. The simulation and experimentation were also conducted by Farhad Fakour.

REFERENCES

1. Liu S. Multi-objective optimization design method for the machine tool's structural parts based on computer-aided engineering. Int J Adv Manuf Technol. 2015;78,:1053-1065.

2. Shen Y, et al. A multi-objective optimization method for forging machine based on genetic algorithm. China Mech Eng. 2012;23:291-294.
3. Liu SH, et al. Design plan optimum seeking of machine tool bed based on grey relational analysis. J Grey Syst. 2010; 22:341-352.
4. Li B, et al. Optimal design of machine tool bed by load bearing topology identification with weight distribution criterion. Procedia CIRP. 2012;3:626- 631.
5. Li BT, et al. Stiffness design of machine tool structures by a biologically inspired topology optimization method. Int J Mach Tool Manu. 2014;8433-44.
6. Abuthakeer SS, et al. Structural redesigning of a CNC lathe bed to improve its static and dynamic characteristics. Annals of Faculty Engineering. Int J Eng Tome IX. 2011;3:389-394.
7. Zhao H, et al. Static and dynamic characteristics analysis of precise composite CNC grinding machine. Adv Mater Res. 2012;411:88-93.
8. Yang H, et al. Static and dynamic characteristics modeling for CK61125 CNC lathe bed basing on FEM. Procedia Engineering. 2017;174:489-496.
9. Duan Y, et al. Improvement design research of a CNC lathe-bed structure. Appl Mech Mater. 2011; 50-51:1028-1032.
10. Saidaiah J, et al. Weight optimization of lathe bed by design modification and epoxy granite. SSRG Int J M Eng. 2017; 4:23-32.
11. Swami BM, et al. Design and structural analysis of CNC vertical milling machine bed. Int J Adv Eng Tech. 2012;3:97-100.
12. Shrivastav A, et al. Optimization of design parameter of vertical machining center column for the weight and rigidity. Int J Adv Eng Res Dev. 2017;4:750-754.
13. Srinivasan S, et al. Design and structural analysis of CNC milling machine bed with composite material. Imperial Journal of Interdisciplinary Research (IJIR). 2016; 2:147-151.
14. Fakour F. Shape optimization tool based on finite element analysis. M.S. Thesis, California State University, Chico, USA. 1994.
15. Finkelstein, A. Understanding mass participation factor results in frequency studies. 2019.
16. Xu G, et al. Study on dynamic characteristics analysis of CNC pipe thread lathe based on the energy of modal effective mass. 2019;13:335-339.
17. Irvine T. Effective modal mass and modal participation factors. 2015.